ACS APPLIED MATERIALS & INTERFACES

Research Article

Cite This: ACS Appl. Mater. Interfaces 2019, 11, 45354−45363

www.acsami.org

Strong Headgroup Interactions Drive Highly Directional Growth and Unusual Phase Co-Existence in Self-Assembled Phenolic Films

Renaud Miclette Lamarche and Christine DeWolf*

Department of Chemistry and Biochemistry and Centre for NanoScience Research, Concordia University, 7141 Sherbrooke St. West, Montreal H4B 1R6, Quebec, Canada

Supporting Information

ABSTRACT: Self-assembled materials as surface coatings are used to confer functional properties to substrates, but such properties are highly dependent on molecular organization that can be controlled through tailoring the noncovalent interactions. For monomolecular films, it is well-known that strong, dipolar interactions can oppose line tension generating noncircular domain growth. While many surfactant films exhibit liquid crystalline arrangement of the alkyl chains, there are relatively few reports of crystalline headgroups. Here, we report the self-assembly of phenolic surfactants where the combination of hydrogen bonding and π-stacking leads to a herringbone arrangement of the headgroups, generating a molecular super-lattice that can be observed using grazing incidence X-ray diffraction; such an arrangement has been previously proposed for related phenolic systems but never experimentally observed. We also investigated using pH to modulate the intermolecular interactions and the response of the system in terms of molecular organization. The first hydroxyl deprotonation does not appear to impact the structure but has significant impact on the domain size and morphology. Higher pH generates both strong directional domain growth and a loss of the molecular lattice structure, attributed to a second deprotonation. In contrast, a shorter chain surfactant, lauryl gallate, forms a liquid expanded phase that can contract upon deprotonation. In the condensed phase, the deprotonation kinetics are unusually slow for which an internal charge re-organization is proposed. The slow kinetics leads to the co-existence of three distinct phases for a single component system over relatively long timescales and provides evidence of a liquid-mediated polymorphic transformation process in two-dimensional, soft-matter films. This work has implications for understanding the long-range ordering in aromatic self-assembled structures and the mechanisms underlying Langmuir monolayer polymorphism.

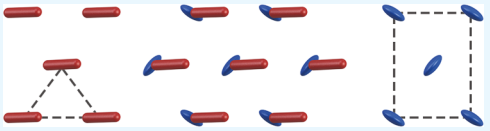

KEYWORDS: *phenol, GIXD, Langmuir monolayer, crystalline headgroups, protonation state, herringbone packing, molecular lattice*

INTRODUCTION

Polyphenols such as tannins exhibit antioxidant, protein binding, and metal chelating properties.[1] The latter is dependent on the orientation and proximity of multiple phenol moieties.[2] Phenolic surface coatings may confer such properties to a substrate, and it may be possible to tune the reactivity and specificity by modifying the distance between phenols. While it is possible to control the distance by synthesizing polyphenols with specific arrangements, an alternative method would be to control the intermolecular distance in self-assembled films using phenolic-derived building blocks. For example, long-chain phenolic surfactants and lipids have been shown to self-assemble at liquid[3] and solid surfaces.[4] In this work, we seek to control the domain morphology and intermolecular distances in Langmuir monolayers at the air−water interface; such films could subsequently be deposited onto solid substrates as coatings to harness the phenol properties.

The organization of surfactants at the air−water interface is determined by noncovalent interactions. The interplay of hydrogen bonding, ion−dipole and/or dipole−dipole[5,6] interactions, and π-stacking[7] are shown to modify the structure and morphology of surfactant films. Phenol headgroups afford the opportunity to modify each of these which in turn can be used to tune the interphenolic distance. With more than one hydroxyl on the headgroup, the charge can be varied systematically, inducing either attractive or repulsive interactions. Additionally, the hydrophobic tail can be modified by changing the length and the number of branches, while the headgroup interactions can be altered by changing the subphase composition. For example, the addition of ions to the subphase, either as part of the effort to modify the pH of the subphase or by deliberately adding salt, can also modify the interaction with ions influencing the monolayer behavior.[8]

Our group has previously reported the monolayer properties of a phenol lipid, dipalmitoylgalloylglycerol, and found evidence of a highly cohesive and rigid film attributed to an extensive hydrogen bond network between the phenol headgroups which comprise multiple hydroxyl groups.[9] Peikert et al.[10] studied phenolic surfactant films with variation in the hydroxyl position. Using grazing incidence X-ray diffraction (GIXD) and computational methods, they determined possible arrangements of the headgroups where the aromatic ring can interact with four adjacent rings, maximizing the π-stacking interactions, hinting that despite the weakness of the π-stacking relative to hydrogen bonding, this can still

Received: September 18, 2019
Accepted: November 11, 2019
Published: November 11, 2019

DOI: 10.1021/acsami.9b16958
ACS Appl. Mater. Interfaces 2019, 11, 45354−45363

significantly influence the organization of the monolayer. Studies of phenol-terminated self-assembled monolayers (SAMs) showed that simply changing the hydroxyl group from the meta- to the para-position can lower the surface coverage of the deposited SAM by 40−60%, attributed to a modification of the organization at the interface.[11] Not only the position of the hydroxyl on the ring but also the protonation state affects the orientation and exposure of the headgroup and hence the hydrophilicity of the film surface.[11] Azmi et al.[12] showed that the relative hydroxyl positions (1,2- or 1,3-) of dihydroxyphenol-terminated SAMs determined the intermolecular hydrogen bonding that impacted the extent of binding of the phenolic SAMs with phosphate. Specifically, the 1,2-diol had significantly higher binding potential to monoprotic phosphate, attributed to the ability of the 1,3-diol to hydrogen bond with multiple neighboring surfactants, reducing the binding potential to the phosphate.

In the present work, the self-organization of two phenolic surfactants, lauryl gallate (LDG) and octadecyl gallate (ODG) (Figure 1), which differ only in the length of their chains, are

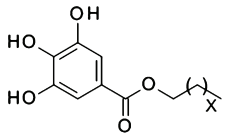

Figure 1. Structure of surfactants used, X = 10 LDG, X = 16 ODG.

studied as a function of monolayer subphase composition. The difference in the chain length enables determination of the impact of suphase pH and ionic strength as a function of the phase of the film (liquid-expanded vs condensed) while maintaining the same headgroup. The two phases afford different routes to controlling the intermolecular spacing that will be required for applications involving protein and metal binding.

The organization of phenol surfaces and interfaces is relevant for understanding systems as diverse as the interaction of aqueous phosphates with phenolic-rich natural-organic matter (humic material)[12] to natural and synthetic cross-linked biopolymer materials including the adhesion of mussels[13] and protein binding.[14] A recent review highlighted the importance of phenolic building blocks for the assembly of functional materials.[15] Amphiphilic phenols provide an opportunity to tailor the self-assembly of materials via modifications in the arrangement of functional moieties on the headgroup, and electrostatic contributions to hydrogen bonding (H-bonding) affect film organization, properties, and structure.

MATERIALS AND METHODS

Materials. LDG (≥99.0%) was purchased from Sigma-Aldrich and used without further purification. ODG was synthesized from gallic acid and octadecanol using para-toluene sulphonic acid[16] under reflux conditions and recrystallized from chloroform and hexane. Ultrapure water (resistivity of 18.2 MΩ/cm) was obtained from an EASYpure II LF system (Barnstead, Dubuque IA). The spreading solutions were prepared using chloroform (HPLC grade, trace of ethanol as preservative) from Fisher Scientific company. Mica (grade V1) used in the atomic force microscopy (AFM) deposition was purchased from Ted Pella Inc. and freshly cleaved before each measurement.

Isotherm Measurements. Monolayers were spread from a chloroform spreading solution (1−1.5 mM) on three different types subphases: (i) ultrapure water (pH = 5.5 at 25 °C), (ii) ultrapure water that was adjusted to higher pH using NaOH, (iii) ultrapure water that was ionic strength-adjusted using NaCl. Surface pressure−area isotherms were obtained on Langmuir film balances (Nima Technology Ltd., Coventry, U.K.) at room temperature with a compression speed of 5 cm^2/min (equivalent to between 3 and 7 $Å^2$/molecule·min depending on spreading solution concentration). Two different Langmuir film balances were used, one with a dimension of 5 cm by 35 cm was used for LDG isotherms and Brewster angle microscopy (BAM) and the other had dimensions of 7 by 15 cm and was used for ODG isotherms. Surface pressure measurements were made using a filter paper Wilhelmy plate (Whatman no. 1 paper). Monolayers were given 10 min for film relaxation unless stated otherwise. Monolayers were transferred at a constant pressure onto mica on the upstroke using the Langmuir−Blodgett technique with a dipping speed of 1 mm/min. All transfer ratios were always close to 1. Compressibility modulus measurement was calculated using[17]

$$C_s = -\frac{1}{A}\left(\frac{\partial A}{\partial \pi}\right)_T$$

Brewster Angle Microscopy. BAM was carried out with an I-Elli2000 imaging ellipsometer (Nanofilm Technologies GmbH, Göttingen, Germany) equipped with a 50 mW Nd:YAG laser (λ = 532 nm). All experiments were performed using a 20× magnification with a lateral resolution of 1 μm. BAM experiments were performed at an incident angle of 53.15° (Brewster angle of water) and a laser output of 50% (analyzer, compensator, and polarizer were all set to 0).

Atomic Force Microscopy. A Nanoscope IIIa (Digital Instruments, Santa Barbara, CA) was used to capture AFM images in air at room temperature using a tapping mode at a scan rate of 1 Hz using etched silicon cantilever frequency of ∼300 kHz, a nominal spring constant of 20−80 N/m, and a tip radius of <10 nm. An oscillation amplitude of 175 mV and medium damping (∼25%) were employed for these measurements.

Grazing Incidence X-ray Diffraction. The GIXD experiments were performed at beamline 15-ID-C ChemMatCARS at the Advanced Photon Source (APS) in Argonne National Laboratory with the following parameters: X-ray beam wavelength of 1.239 Å, incidence angle of 0.09061, horizontal size of 20 mm, and vertical size of 120 mm, leading to a beam footprint of 20 mm by 7.6 cm. The detector used was the two-dimensional Swiss light source PILATUS 100K set to the single-photon counting mode. Two sets of slits, one placed in front of the detector and the other placed 280.0 mm from the sample, were used to minimize intense low-angle scattering. Experiments were performed at the air/water interface of a 340 cm^2 Langmuir trough, where the monolayer was spread and then compressed at rates of 2 and 5 cm^2/min (equivalent to 0.5 and 1.3 $Å^2$/molecule·min, respectively) using a mobile barrier. The measured GIXD data are plotted as contour plots of the intensity as a function of both the horizontal (Q_{xy}) and the vertical (Q_z) scattering vector components. The lattice spacing d_{hk} was obtained from the in-plane diffraction data as $d_{hk} = 2\pi/q_{xy}^{hk}$, where the Miller indices h and k were used to index the Bragg peaks needed to calculate the unit cell parameters for the in-plane lattice.[18,19] Raw data were extracted and patched using software developed by Wei Bu, beamline scientist at ChemMatCARS. The Bragg rods and peaks were fitted with the Gaussian and Lorentzian function, respectively, using Origin lab graphing and analysis software.

RESULTS AND DISCUSSION

The isotherm of ODG on ultrapure water (pH 5.5) exhibits a sharp increase in surface pressure at areas below 30 $Å^2$/molecule (critical area for onset of surface pressure), indicative of the formation of a condensed phase (blue isotherm, Figure 2). The surface pressure increases without evidence of phase transition until film collapse at an area of 23 $Å^2$/molecule and 50 mN/m. The film morphology was visualized using BAM (Figure 3a). Already at high molecular areas and 0 mN/m

DOI: 10.1021/acsami.9b16958
ACS Appl. Mater. Interfaces 2019, 11, 45354−45363

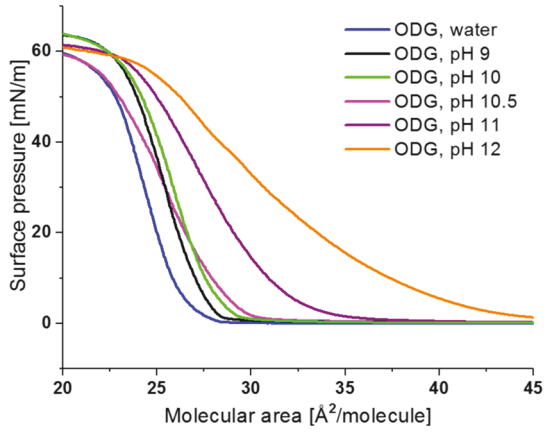

Figure 2. Surface pressure−molecular area isotherms of ODG as a function of subphase pH.

surface pressure, large, condensed phase domains are visible, an indication of the strong intermolecular interactions between the headgroups. The domains are untextured (isotropic) and separated by dark regions that comprise either gaseous phase. If the solution is sonicated for 15 min before spreading, the domains seen are smaller, but the isotherm does not change. The pressure increases only after the domains are compressed to the point of contact. Most of the domains coalesce producing large regions of the isotropic condensed phase that are larger than the field of view. Periodically, when the interstitial spaces between the domains appear in the field of view, smaller domains of the same condensed material are visible, likely generated by compression of these interstitial spaces by the highly rigid large domains (see Figure 3a). These smaller domains coexist with residual holes. Deposition of the monolayer onto mica by Langmuir−Blodgettry and analysis by AFM reveals clusters of small domains (Figure 4a) that are approximately 1.2 nm above the background. Given the area coverage and the size of the domains observed by BAM and the lack of domains in this size range by AFM, it is presumed that the large, rigid domains break apart upon transfer.

In order to determine the tilt angle and lattice parameters of the condensed phase formed, GIXD measurements were carried out at different pressures (Figure 5a and Table 1) and multiple diffraction peaks were observed. Two are located in the region normally associated with the first order peaks of the alkyl chain lattice, at Q_{xy} 1.28 and 1.63 Å $^{-1}$ (fitted peak positions and widths are provided in the Supporting Information, Table S1); additional peaks were observed at Q_{xy} 1.86 and 0.96 Å $^{-1}$ (Figure S2), and the low Q_{xy} peak will be discussed later. Using these peak positions to characterize the packing of the alkyl chains yields a centered rectangular unit cell with herringbone backing of the alkyl chains (lattice parameters are shown in Table 1). Notably, the unit cell and alkyl chains tilt angle does not change significantly as the film is compressed, suggesting that the molecules adopt a preferred orientation and organization already in the condensed phase domains formed immediately after spreading, and compression serves only to remove the residual gaseous phase regions. This is consistent with the isotherms that do not show evidence of phase transitions.

Analysis of the distortion as a function of $\sin^2 t$ (tilt angle) enables extrapolation of d_0, the distortion at the zero tilt angle.[5,20−22] This analysis for ODG shows a nonzero value of d_0 at 0, indicative of the herringbone arrangement[18,21] of the alkyl chains (Figure S3) which also correlates well with the high Q_{xy} position for the peak at 1.64 Å^{-1}. The peaks observed at Q_{xy} 0.96 and 1.86 Å^{-1} correspond to the $[1,0]_r$ and $[1,2]_r$ peaks, respectively, with the peaks at Q_{xy} 1.28 Å^{-1} and Q_{xy} 1.63 Å^{-1} being indexed as $[1,1]_r$ and $[0,2]_r$, where the "r" subscript denotes the rectangular cell indices (Figure S4 for indexed peak). However, the peak at Q_{xy} 1.86 Å^{-1} can only be fit with a full width at half maximum (fwhm) in the Q_z direction of 1.05 Å^{-1} (intensity in the Q_z direction in Figure S5), which corresponds to a scattering rod length of 5.4 Å,[23] whereas the other peaks exhibit a fwhm of 0.28 Å^{-1} in better agreement with a tilted C18 chain. In the absence of any other phases, and given the large fwhm, this reflection is proposed to be the result of an organized headgroup layer. Such an organization was proposed based on simulations for ether-linked, mono- and di-hydroxy phenolic surfactants but not observed by GIXD.[10] Organization of the headgroup leads to the possibility that the centered rectangular herringbone arrangement arises because of a molecular lattice with a nonequivalent headgroup orientation. If the alkyl chains were also to be in the herringbone arrangement, a corresponding strong $[1,2]_r$ peak should be observed at the same Q_{xy} = 1.86 Å^{-1}, but such a peak would need to be out-of-plane because of the tilting of the chain. We cannot preclude that this peak is buried under the large width peak at 1.86 Å^{-1} (Figure S5) and that the chains are also in a herringbone arrangement as might be expected given the A_0 (chain area normal to the long axis) is 19.2 Å^2, significantly less than the 20−21 Å^2 required for orientational disorder (the free-rotator phase). Notably, most reports of single chain surfactants of similar length that adopt a herringbone arrangement of the alkyl chains are for temper-

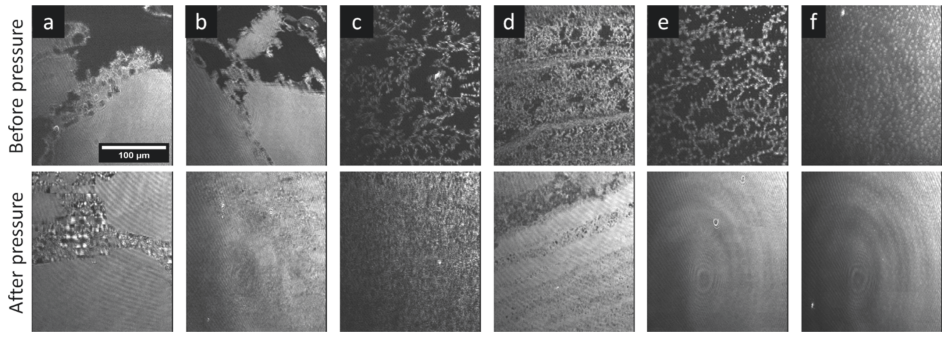

Figure 3. BAM images of ODG, before and after the onset of pressure on various subphases with 10 min relaxation time: (a) water, (b) pH 9, (c) pH 10, (d) pH 10.5, (e) pH 11, (f) pH 12.

DOI: 10.1021/acsami.9b16958
ACS Appl. Mater. Interfaces 2019, 11, 45354−45363

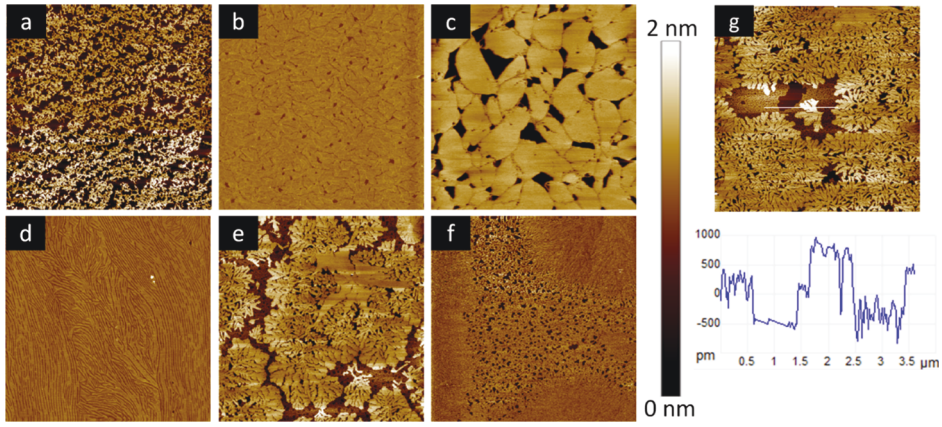

Figure 4. AFM images of ODG monolayers deposited by Langmuir−Blodgettry onto mica substrates at a pressure of 1 mN/m with 10 min relaxation. Subphase and image sizes are as follows: (a) water, 20 μm, (b) pH 9, 5 μm, (c) pH 10, 15 μm, (d) pH 10.5, 15 μm, (e) pH 11, 10 μm, (f) pH 12, 10 μm, (g) pH 11, 10 μm with height scan underneath.

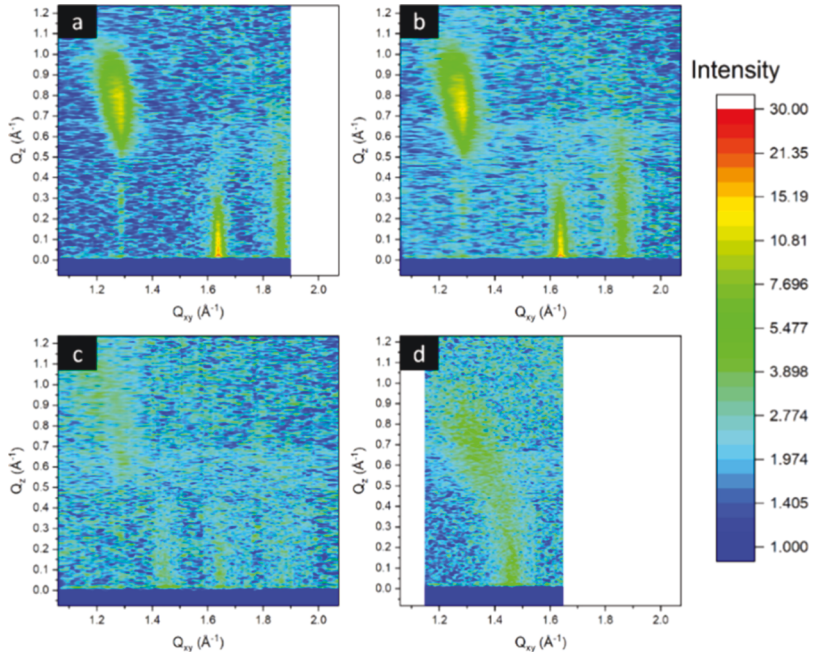

Figure 5. GIXD contour plot of X-ray intensity as a function of the in-plane (Q_{xy}) and out-of-plane (Q_z) vector components for ODG on : (a) water, 5 mN/m (b) pH 9, 5 mN/m (c) pH 11, with 10 min relaxation time, 20 mN/m (d) pH 11 with 60 min relaxation time 5 mN/m.

atures significantly below room temperature. There is a report of a herringbone structure at higher temperature for a longer chain length (C22) for which high surface pressures are required.[24] Therefore, if a herringbone organization of the chains is present, it must be driven by the strong headgroup noncovalent interactions.

Normally, the $[0,1]_r$ and $[1,0]_r$ peaks of a herringbone, centered rectangular unit cell are symmetry forbidden.[25] In this case, a weak $[1,0]_r$ peak is observed at Q_{xy} 0.98 Å^{-1} (Figure S2), but the corresponding $[0,1]_r$ peak predicted to be at 0.8 Å^{-1} was not observed (the full Q_{xy} scan range was from 0.8 to 2.4 Å^{-1}). Böhm et al.[26] observed both [1,0] and [0,1] in the case of stacked multilayers; however, both AFM and BAM exclude this possibility for our system. Thus, the observance of the $[1,0]_r$ peak must derive from form factors in this direction that are not identical because of headgroup orientations. The lack of $[0,1]_r$ either implies that in this direction, the symmetry is maintained and the form factors are still equivalent or the crystallinity in this direction is significantly weaker. Note that the Q_{xy} position of the $[1,1]_r$ peak of the headgroup or molecular superlattice is commensurate with the alkyl chain peak at Q_{xy} 1.28 Å^{-1} which possesses a strong form factor around Q_z 0 Å^{-1} and therefore cannot be explicitly identified.

While herringbone higher order peaks for alkyl chains have been reported since the early 1990's for single chain fatty acids, molecular superlattices derived from strong headgroup organization leading to nonfree rotation of the headgroup are less common. However, the strong intermolecular hydrogen bonding and π-stacking interactions between the gallate headgroups could be sufficient to induce ordering in the headgroup region. Such a hydrogen bond network was previously proposed by Pascher and Sundell[27] in the leaflet of bilayer of sphingolipid, where the hydrogen bond network is inferred from crystal diffraction and by Stefaniu et al.[28,29] for the sugar headgroup ordering in glycosylphosphatidylinositol monolayers. A contributing factor here is the commensurate

DOI: 10.1021/acsami.9b16958
ACS Appl. Mater. Interfaces 2019, 11, 45354−45363

Table 1. Alkyl Chain Unit Cell Parameters Derived from GIXD for ODG at Room Temperature on Various Subphases[a]

pressure (mN/m)	a (Å)	b (Å)	γ (deg)	t (deg)	Ψ
Water					
5	7.66	6.40	90	39	NN
20	7.66	6.37	90	38	NN
40	7.59	6.35	90	37	NN
pH 9 Subphase					
5	7.66	6.40	90	39	NN
20	7.66	6.40	90	39	NN
pH 10 Subphase					
5	7.61	6.37	90	38	NN
20	7.61	6.36	90	38	NN
pH 11 Subphase, 10 min Relaxation Time					
1	7.64	6.40	90	40	NN
20	7.59	6.34	90	35	NN
pH 11 Subphase, 60 min Relaxation Time					
5	8.57	5.11	90	33	NN

[a] a, b, γ are the unit cell dimensions reported using a rectangular unit cell nomenclature, t is the tilt angle relative to normal, and Ψ is the tilt direction relative to the unit cell.

size of the headgroup with that of the single alkyl chain, whereas double chain surfactants or lipids may be bulky enough to keep the headgroups far enough apart to prevent the long-range orientational order.

In order to probe the impact of the headgroup protonation state on this network, experiments were performed over a range of subphase pH values from 7 to 12. Increasing the subphase pH should lead to deprotonation of the phenol and a charged headgroup which would modify the interaction between the surfactants. At pH 7 and pH 8, no discernible changes in the isotherm or morphology were observed (data not shown). At pH 9, the isotherm shifts to higher molecular areas and shows an increased collapse pressure, close to 60 mN/m (Figure 2). There is some disagreement in the literature over the solution pK_a of gallic acid, but there is consensus that the first hydroxyl to deprotonate is the para-position at a pK_a of 8.2[30] or 8.7.[31,32] It is, however, important to note that pK_a is environment-dependent and that the headgroup pK_a in a monolayer can be substantially different from the solution pK_a.[33] Therefore, a modification in isotherm behavior at subphase pH 9 is in reasonable agreement with the deprotonation of the para-hydroxyl. This discrepancy in the literature pK_a values is more pronounced for the meta-positions, with the first position being ascribed three possible pK_a values: 10.4,[32] 10.7,[30] and 11.4[31] and the second meta-position deprotonation also being ascribed a pK_a of 11.4[32] or 13.[30,31] Herein, experiments were not carried out above pH 12, but the isotherms support the idea of a progressive change in the meta-position protonation state over a pH range of 10.5−12 (Figure 2). As might be expected, increasing the extent of deprotonation, and hence the headgroup charge, leads to an expansion of the film because of electrostatic repulsion and consequent shifts to higher molecular areas.

At pH 9, BAM imaging shows a similar morphology as observed on water (Figure 3b); however, the large domains appear more frayed at the edges (Figure S6); the increased repulsion brought about by the deprotonation of the headgroup is most likely weakening the integrity of the domains. Similarly, upon compression, the interstitial spaces never fully coalesce which may be due to the highly rigid nature of the domains and the increased charge. By BAM, these are visible as regions between isotropic domains that are less homogeneous and still contain small holes. AFM of deposited films (Figure 4b) reveals that the large condensed phase regions themselves comprise smaller domains that have not coalesced, evident from the observable grain boundaries and trapped holes comprising either gaseous phase (effectively bare mica). These grain boundaries may induce sufficient flexibility of the film that deposition can occur without the fragmentation that was observed for film transfer from water. Deposition at elevated pressure show that these domains can fuse with each other (Figure S7). Despite the morphological changes, GIXD of ODG on a pH 9 subphase shows an organization almost identical to the one found on ultrapure water (Figure 5b, to be discussed later).

At pH 10 and above, large changes in morphology are observed both at the air−water interface and in deposited films. The large domains seen by BAM at lower pH values are replaced by smaller domains that form a mesh-like structure (Figure 3c). If compressed, they do not coalesce into a uniform condensed phase, instead forming close-packed small domains of various shapes. AFM of films deposited at low pressure (Figure 4c) shows small (<4 μm) distinct domains separated by small regions of the gas phase. This, combined with the BAM and AFM image at higher pressure (Figure S8), indicates that the domains do not fuse even when compressed.

Despite very different morphologies, the isotherms for ODG on pH 9 and pH 10 subphases are very similar. The change in subphase pH is concomitant with a 10-fold change in ionic strength (from 10^{-5} to 10^{-4} M). To investigate this, NaCl was added to a pH 9 subphase such that the concentration of Na^+ ions was the same as for the pH subphase (Figure S9). The isotherm obtained are again similar, but the film morphology resembles that obtained on pH 9 (data not shown), confirming it is the pH changes that alter the morphology and not the ionic strength.

The GIXD measurements yield almost identical lattice parameters for water, pH 9, and pH 10 subphases (Table 1). Therefore, the morphological changes seen by BAM and AFM do not originate from a modification of the surfactant organization and may result from the increase in charge of the domains themselves. As the headgroup becomes deprotonated, the domains will also experience greater interdomain charge repulsion, producing smaller domains that repel hindering coalescence.[34,35] Given the similarity of the isotherms and the Q_{xy} values from GIXD, small domains at subphase pH 10 must generate the same area coverage of the surface as the larger domains at pH 9. Assuming the para-hydroxyl position is the first hydroxyl to deprotonate, as is the case in solution[32] for gallic acid, this could potentially have less impact on a hydrogen bond network that exists between the neighboring surfactant meta-hydroxyls. This would suggest that the meta-positions do not begin to deprotonate until pH > 10.

The BAM morphology comprising chains of small domains persists at pH 11 and becomes more pronounced. The isotherm shifts to significantly higher molecular areas. Unlike pH 10, increasing the pressure leads to a uniform condensed phase in BAM imaging (Figure 3e). However, AFM (Figure 4e,g) reveals a very different internal domain morphology compared to pH 10 (Figure 4c). The domains seen by BAM at 0 mN/m are actually composed of small dendritic, snowflake-

DOI: 10.1021/acsami.9b16958
ACS Appl. Mater. Interfaces 2019, 11, 45354−45363

like features with many branches that continuously split. Grooves are apparent within the dendritic arms (Figure 4g) and have a nominal depth of 0.2 nm, although given their width, this may be tip-limited and thus inaccurate. Typically, the observation of dendritic features coincides with domain formation and growth at a LE−C phase transition plateau[36] which can relax into a circular domain given enough time.[37] Similarly, changing the relative contributions of highly orienting, directional non-covalent interactions (via changing the pH[38] or temperature[39]) versus line tension also impacts dendrimer formation. Careful examination of Figure 4g reveals multiple co-existing phases, the region surrounding the dendrites comprises two phases. The height difference between the dendrites and the lowest phase is approximately 1.0 nm, while the intermediate phase displays a height difference to the lowest phase of 0.7 nm. Periodic holes within the lowest phase confirm that this is not the mica substrate (Figure S10a). It would appear that two different condensed phases are formed and that these co-exist with a liquid-expanded phase. In agreement with BAM imaging, the AFM of a film deposited at 20 mN/m (Figure S10b) shows that the coexistence persists over the timescale of an isotherm, although the phases does begin to coalesce.

The co-existence of multiple phases was studied using GIXD. The diffraction pattern for ODG on a pH 11 subphase shows peaks associated with multiple diffraction patterns. One set of peaks appears at the same approximate positions as observed at the lower pH values (peaks at Q_{xy} 1.28, 1.64 and 1.86 Å^{-1}), although the peaks are significantly weaker. Additionally, the data show the appearance of a new set of peaks (Figure 5c) corresponding to a phase with a lower tilt angle (peaks at Q_{xy} 1.35 and 1.46 Å^{-1}) that yield the unit cell parameters listed in Table 1 for the 60 min relaxation time (note that the unit cell is non-herringbone and centred rectangular). The co-existence of two phases was observed both at low (1 mN/m) and high (20 mN/m) pressures. Notably, the height difference between the two condensed phases obtained by AFM was 0.3 nm, which corresponds well to the estimated height difference for chains tilted at 40 and 33°.

According to the Gibbs phase rule, in a one component system, multiple thermodynamically stable phases can theoretically only coexist at phase transitions but not over broad ranges of surface pressures. In practice, the phase transition can be broader than a single surface pressure as the compression speed renders the film not at thermodynamic equilibrium. However, such coexistence over broad ranges of surface pressures could be due to a slow rearrangement of the surfactant because of the increase in pH or separation into two phases, one rich in the deprotonated component and one rich in the protonated component. To test this, the film was allowed to relax for 60 min prior to compression. This shows a complete loss of the peaks associated with the higher tilt angle phase (Q_{xy} 1.28 and 1.64 Å^{-1}) and an increased intensity for the lower tilt angle phase (Figure 5d). This relaxation of the film also induces a change in the isotherm to higher molecular areas (Figure S11). Film relaxation also alters the morphology observed by BAM with rounder, larger domains that never fully coalesce (as indicated by the residual holes at high pressure, Figure 6c), hence the shift is to larger average molecular areas, despite a lower tilt angle. In agreement with GIXD, AFM (Figure 6d) confirms that relaxation yields a film comprising only two distinct heights, attributed to a single condensed

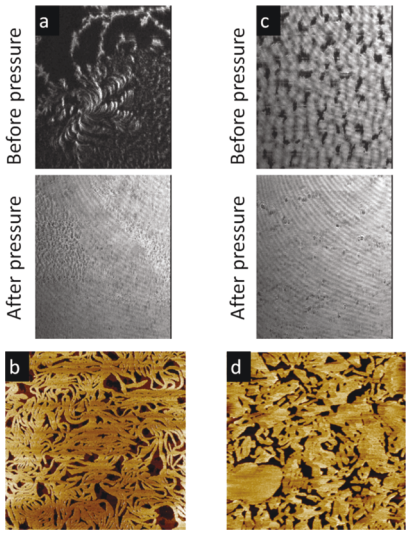

Figure 6. BAM and AFM of ODG after 60 min relaxation time at subphase pH 10.5 (ab) (size of 10 μm, deposition at 1 mN/m) and pH 11 (cd) (size of 5 μm, deposition at 1 mN/m).

phase with a surrounding low density region (gaseous phase). These results confirm that the multiple phases arise from slow kinetics rather than impurities.

Hossain et al. saw similar dendritic features by BAM for a monolayer of di-*n*-dodecyl hydrogen phosphate which, upon equilibration at constant pressure, relaxed into circular-shaped domains.[37] In our case, the dendritic phase is the less tilted (higher) phase and appears to grow initially at the expense of the more tilted (lower) phase. This less tilted phase exhibits a fast initial dendritic growth that is not kinetically stable and thus, as the film relaxes, the dendrites re-organize to form more rounded domains, highlighting the competition between directional growth due to strong intermolecular interactions and line tension. Notably, the phase that emerges upon relaxation of the film no longer exhibits the high crystallinity or the herringbone packing observed at lower pH values (Figure 5a,d). Keeping in mind that the pK_a for the second deprotonation in the meta-position has been reported to be in the range of 10.4−11.4 and assuming the para-hydroxyls to already be majority deprotonated,[32] these changes are likely attributable to a second deprotonation, that is, deprotonation of the one of the meta-hydroxy groups. Given the film is spread from chloroform into a highly aggregated state (at high molecular areas) onto a subphase of high pH, one has to assume a component of the kinetics is the rate of deprotonation which would require disrupting existing strong interactions, keeping in mind that in a condensed film, the gallate cannot be considered in dilute solution. The second component that must be considered is a potential re-organization from the deprotonation in the para- and meta-positions to deprotonation at both meta-positions which would limit the internal charge repulsion and alter the headgroup dipole. The former (para-/meta-deprotonated) has a strong headgroup dipole which could have a preferred growth direction and could explain the dendritic growth pattern, while the latter (meta-/meta-deprotonated) has no net headgroup dipole thus could result in the line-tension dominated, circular domains. Transfer from one phase to another must occur via dissolution from the domain edges into an intermediate liquid-expanded phase as observed by AFM, a

DOI: 10.1021/acsami.9b16958
ACS Appl. Mater. Interfaces 2019, 11, 45354−45363

process similar to the concept of Ostwald ripening or solution-mediated polymorphic phase transformation.

In order to probe this pH-induced transition, an intermediate pH value of 10.5 was also studied and also shows the time-dependent reorganization. Branching and spiral patterns are visible by BAM and AFM (Figure 6a,b) supporting the proposed second deprotonation around this pH. If the film is compressed with minimal wait time, the domains clearly coalesce into long, highly oriented, striated regions (Figure 3d). Compression after longer relaxation time (Figure 6a) generates a greater coverage in the uniform condensed phase, although areas resembling the smaller domains observed for pH 10 persist. AFM imaging (Figure 4d) also shows a highly striated film, although on a completely different length scale. The observed crevasses are of varying length and average 0.4 nm deep, although again, this depth measurement is likely tip-limited because of their small lateral size. Clearly, strong orienting headgroup interactions dominate over line tension in defining the domain shape. The lack of coalescence of these long domains is likely due to increased repulsion between surfactant domains.[34] The lower proportion of di-deprotonated headgroups mixed with the mono-deprotonated would then generate elongated, strand-like domains even after relaxation (Figure 6b). This also demonstrates that the changes observed at pH 11 with long relaxation times are not due to the small change in pH from CO_2 absorption, which will lower the pH, because longer relaxation times at pH 11 lead to rounder domains, not long striated ones. The proposed deprotonation states and associated molecular re-organizations, both within the molecule and within the film, leading to this phase behavior are under investigation using computational methods.

At pH 12, multiple small bright domains are visible by BAM (Figure 3f) although there do not appear chains of domains forming. Notably, the contrast between the domains and the continuous matrix is significantly reduced. As the pressure increases, this background gets brighter until it is the same brightness as the small circles and the morphology become homogenous. AFM reveals that the domains seen by BAM are regions of higher density of the condensed phase, and these are also dendritic in appearance, especially at the edges, but they are visibly distinct from those seen at pH 11. These are surrounded by regions of small nanodomains co-existing with the gas phase; hence, the similarity in optical properties to the domains which causes the low BAM contrast. As the pressure increases, the visible holes, which are trapped remnants of the gas phase, are eventually excluded as the film fully coalesces, leading to full loss of contrast in BAM. GIXD measurements indicate that only the lower tilt angle phase (seen at pH 11 with long relaxation time) is formed with no evidence of the higher tilt angle phase or headgroup ordering (data not shown). The structure is not included in Table 1 because the peaks, although evident, are too weak to be fit accurately. Given the amount of the condensed phase found by AFM imaging, the weaker peaks must be attributed to extremely low correlation lengths. The presence of only one phase (low tilt angle) indicates that at higher pH, the rate of deprotonation and kinetic re-arrangements increases. Time-dependent studies were performed but show no change to the morphology or structure, indicating that this polymorph is stable for relaxation times up to 12 h.

The impact of pH on the film properties is clearly mapped in the compressibility modulus as a function of pH (Figure 7). Three distinct regimes are observed that, according to our proposed model, would correlate with (i) predominantly protonated and mono-deprotonated (water, pH 9, pH 10), (ii) mixed mono- and di-deprotonated (pH 10.5, pH 11), and (iii) predominantly di-deprotonated (pH 12) headgroups. The first two regimes correspond in compressibility moduli to condensed phases,[17,40] (C_s > 200 mN/m in all cases), however, as the charge repulsion of domains increases and hinders full coalescence, the compressibility modulus decreases.

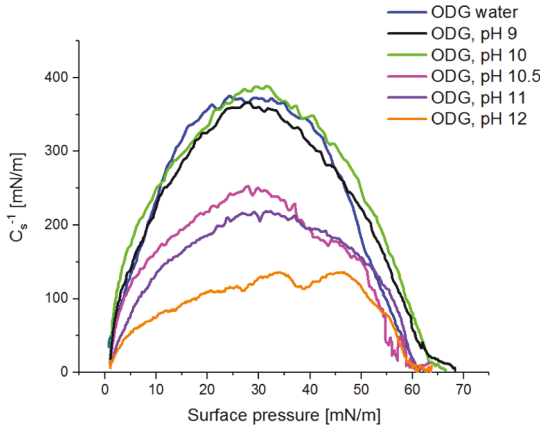

Figure 7. Compressibility modulus of ODG as a function of subphase pH.

In order to determine the effect of the chain length on the pH-induced phase behavior, a shorter analogue, LDG, was studied. LDG films on ultrapure water exhibit an isotherm typical of a liquid-expanded phase (Figure 8) with a critical area for pressure onset at 55 Å^2/molecule. It remains in this phase until film collapse at 20 Å^2/molecule and 47 mN/m. This collapse area is larger than that of ODG, but not significantly, suggesting that there may be some solubility of LDG in the subphase which has been reported for surfactants with a C12 alkyl chain.[41] AFM measurements of films deposited by the Langmuir–Blodgett method on mica confirm a single phase with a flat, featureless surface (data not shown). As a result, the headgroups should not be in such close proximity as observed with ODG. In contrast to ODG for which the headgroup deprotonation at pH 9 induces a shift of the isotherm, there is no significant change in the molecular

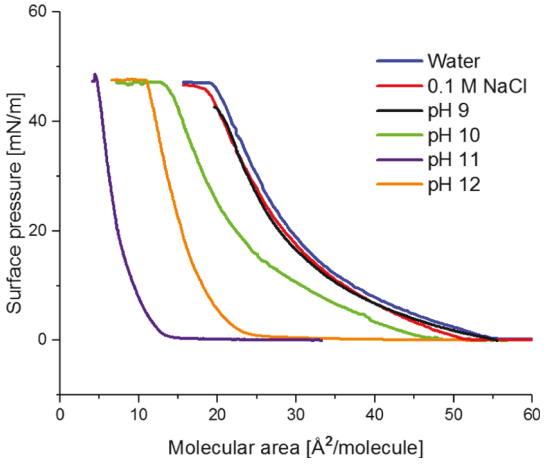

Figure 8. Surface pressure–molecular area isotherms of LDG as a function of the subphase.

DOI: 10.1021/acsami.9b16958
ACS Appl. Mater. Interfaces 2019, 11, 45354–45363

area for LDG at pH 9 compared to ultrapure water (Figure 8). Similarly, the addition of 0.1 M NaCl has no impact on the widely spaced headgroups, whereas with the close-packed ODG, insertion of the counterion into the headgroup region expanded the film (Figures 8 and S9). The first significant change in the isotherm area occurs at pH 10 (for ODG the first noticeable shift was observed at pH 9). This may result from one of two factors, either the greater headgroup spacing enables water and counterion screening of the charge on the para-hydroxy and weakens the electrostatic repulsion or there is a difference in the first pK_a because of the differences in the phase. Notably, the isotherm shifts to smaller molecular areas in contrast to ODG which exhibited a shift to higher molecular areas with increasing pH. In this case, deprotonating the para-position generates an ion−dipole interaction which is strong enough to bring the molecules closer together, whereas in ODG, the charge repulsion in a close-packed system generates an increase in the molecular area.

At pH 11, there is a larger shift to smaller molecular areas, this time accompanied by a change in isotherm shape; it would be expected that the isotherm exhibits a change in compressibility modulus,[17] corresponding to a condensed phase, however, there is no apparent change when compared to a film on ultrapure water (Figure 9). Given the molecular

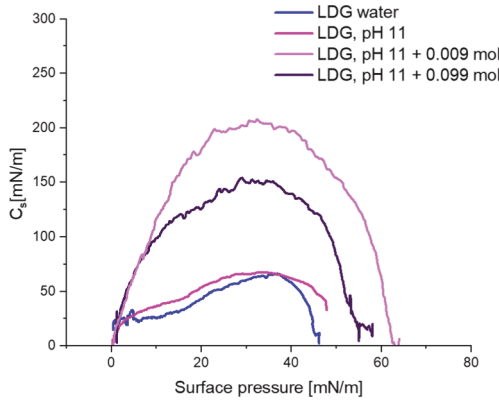

Figure 9. Compressibility modulus of LDG as a function of the subphase; NaCl was added to increase the ionic strength of the subphase to be equivalent to the subphase of higher pH.

area values are lower than what can be reasonably expected for a single alkyl chain,[42] this suggests that the films is not a true insoluble monolayer and that at this pH, solubility becomes a significant factor, which is reflecting in the compressibility modulus remaining that of a liquid expanded phase despite the low apparent molecular area. To counter the effect of solubility, the subphase salt concentration and ionic strength was increased to reduce the surfactant dissolution.[43] Figure S13 shows the isotherms for LDG isotherm at pH 11 with sufficient NaCl to bring the ionic strength equivalent to that of the subphase adjusted to pH 12 (0.01 M) and 13 (0.1 M) with NaOH. These isotherms result in a clear increase in the compressibility modulus which is highest for pH 11 with 0.01 M NaCl. This supports the idea that the ion−dipole headgroup interactions are, at this pH, bringing the headgroups closer together because the addition of counterions into the headgroup region expands the film.[44]

Despite the condensing effects noted, no discernible features were observed using BAM (data not shown). To ascertain whether or not a condensed phase is formed, the monolayer was deposited by Langmuir−Blodgettry onto mica at 1 mN/m for characterization using AFM (Figure S14). Unlike the deposition at neutral pH, the film is not homogeneous but rather exhibits a large number of small holes with an average depth of 0.5 nm and diameter of only a few nanometers. It is not clear if the holes are present at the air−water interface or if they are induced by the transfer as these features are too small to be observed by BAM. Transferring the monolayer at higher pressure, 30 mN/m, leads to a smooth surface (data not shown).

Isotherms on a pH 12 subphase show a critical area intermediate between that on water and on a pH 11 subphase (Figure 8). As was seen at pH 11 and high salt concentrations, the ionic strength of pH 12 (0.01 M NaOH) will limit the solubility of the surfactant; this reduction in solubility accounts for the difference in isotherms between pH 11 and 12. This is reinforced by AFM imaging of a film deposited from a pH 12 subphase which shows a topology very similar to that seen at pH 11 (Figure S14).

CONCLUSIONS

The air−water behavior of the monolayer comprising a phenolic surfactant was investigated as a function of the subphase pH and chain length. ODG on all subphases up to pH 10 exhibits evidence of strong headgroup ordering both in the morphology (high aggregation at high molecular areas) and structure, as revealed by GIXD measurements. For the latter, additional peaks were attributed to a molecular superlattice which exhibits herringbone packing of the headgroups but not necessarily the alkyl chains. Initial deprotonation, presumed to be the para-position, has no impact on the intermolecular organization and structure but does impact morphology as revealed by BAM and AFM. As domain acquires a greater charge, they become smaller and resist coalescence because of inter-domain electrostatic repulsion. At high pH, a second deprotonation is presumed to occur because stronger impacts on morphology, structure, and relaxation time are observed. Because of the slow kinetics of re-organization, multiple phases are observed to co-exist over a broad range of surface pressures. This has been attributed to the kinetics of deprotonation in a condensed phase and possible internal re-distribution of the internal charges on the headgroup. The generation of a strong headgroup dipole favors highly directional growth in films containing the proposed di-deprotonated headgroup, at the expense of line tension. Moreover, the greater charge promotes the loss of the molecular superlattice organization seen at lower pH in favor of a very different unit cell that does not show signs of herringbone packing. To our knowledge, the impact of strong orientational ordering of headgroups has not previously been shown to affect the kinetics of deprotonation and resulting phase behavior in Langmuir monolayers. Notably, the hindrance of deprotonation due to the crystalline headgroup region, leads to an unusual condensed phase growth mechanism in which the kinetics of the system leads to the formation of a liquid phase as an intermediate in the transition from one condensed phase to another. This is in effect a 2D analogy to the transformation between different polymorphs in the presence of a mother liquor, except that in this case the mother liquor is not a solvent but rather a liquid form of the same material.

In contrast to ODG, initial deprotonation of the para-hydroxyl of LDG, which forms a liquid-expanded phase on

DOI: 10.1021/acsami.9b16958
ACS Appl. Mater. Interfaces 2019, 11, 45354−45363

water because of the decreased van der Waals interactions, leads to a film contraction due to the increase in headgroup interaction strength, brought about due to the replacement of dipole−dipole interaction with stronger ion dipole. This demonstrates how the same modification, deprotonation, can have very different impacts on a monolayer depending on the monolayer phase. The ability to use subphase pH and the chain length to finely tune the intermolecular interactions, headgroup dipole moments, and line tension provides the means to easily access a variety of domain morphologies even while keeping the internal structure the same. Understanding interplay of such thermodynamically and kinetically driven processes will guide the design of new building blocks for functional surface coatings and self-assembled structures.

■ ASSOCIATED CONTENT

Supporting Information

The Supporting Information is available free of charge at https://pubs.acs.org/doi/10.1021/acsami.9b16958.

Fitted data of the GIXD peak, additional representation of the peak associated with the supramolecular lattice, distortion analysis, AFM of deposition at higher pressure along with deposition of LDG at pH 11, and additional BAM images for selected systems (PDF)

■ AUTHOR INFORMATION

Corresponding Author

*E-mail: Christine.dewolf@concordia.ca.

ORCID

Christine DeWolf: 0000-0002-5185-7237

Author Contributions

The manuscript was written through contributions of all authors.

Notes

The authors declare no competing financial interest.

■ ACKNOWLEDGMENTS

C.D. acknowledges funding from the Natural Sciences and Engineering Research Council (NSERC) of Canada and the Canada Foundation for Innovation (CFI). R.S. and C.D. are members of the multi-institutional Québec Center for Advanced Materials (QCAM).We thank Michel Goldmann for discussion of the GIXD interpretation and Rolf Schmidt for discussion on the isotherm, BAM and AFM. The ODG synthesis was carried out by Joseph Carrigan. NSF's ChemMatCARS Sector 15 is principally supported by the Divisions of Chemistry (CHE) and Materials Research (DMR), National Science Foundation, under grant number NSF/CHE-1834750. Use of the Advanced Photon Source, an Office of Science User Facility operated for the U.S. Department of Energy (DOE) Office of Science by Argonne National Laboratory, was supported by the U.S. DOE under contract nNo. DE-AC02-06CH11357.

■ REFERENCES

(1) Quideau, S.; Deffieux, D.; Douat-Casassus, C.; Pouységu, L. Plant Polyphenols: Chemical Properties, Biological Activities, and Synthesis. *Angew. Chem., Int. Ed.* **2011**, *50*, 586−621.

(2) Baxter, N. J.; Lilley, T. H.; Haslam, E.; Williamson, M. P. Multiple Interactions between Polyphenols and a Salivary Proline-Rich Protein Repeat Result in Complexation and Precipitation. *Biochemistry* **1997**, *36*, 5566−5577.

(3) Moehwald, H.; Brezesinski, G. From Langmuir Monolayers to Multilayer Films. *Langmuir* **2016**, *32*, 10445−10458.

(4) Czolkos, I.; Jesorka, A.; Orwar, O. Molecular Phospholipid Films on Solid Supports. *Soft Matter* **2011**, *7*, 4562−4576.

(5) Johann, R.; Brezesinski, G.; Vollhardt, D.; Möhwald, H. The Effect of Headgroup Interactions on Structure and Morphology of Arachidic Acid Monolayers. *J. Phys. Chem. B* **2001**, *105*, 2957−2965.

(6) Johann, R.; Vollhardt, D.; Möhwald, H. Study of the PH Dependence of Head Group Bonding in Arachidic Acid Monolayers by Polarization Modulation Infrared Reflection Absorption Spectroscopy. *Colloids Surf., A* **2001**, *182*, 311−320.

(7) Fang, L.; Park, J. Y.; Ma, H.; Jen, A. K.-Y.; Salmeron, M. Atomic Force Microscopy Study of the Mechanical and Electrical Properties of Monolayer Films of Molecules with Aromatic End Groups. *Langmuir* **2007**, *23*, 11522−11525.

(8) Kundu, S.; Langevin, D. Fatty Acid Monolayer Dissociation and Collapse: Effect of PH and Cations. *Colloids Surf., A* **2008**, *325*, 81−85.

(9) Schmidt, R.; DeWolf, C. E. Monolayer Behavior of 1,2-Dipalmitoylgalloylglycerol, a Synthetic Lipid with Strong Cohesive Properties. *Langmuir* **2004**, *20*, 3284−3288.

(10) Peikert, M.; Chen, X.; Chi, L.; Brezesinski, G.; Janich, S.; Würthwein, E.-U.; Schäfer, H. J. Phase Behavior and Molecular Packing of Octadecyl Phenols and Their Methyl Ethers at the Air/Water Interface. *Langmuir* **2014**, *30*, 5780−5789.

(11) Taylor, C. D.; Anderson, M. R. Self-Assembled Monolayers of Positional Isomers of (12-Mercaptododecyloxy)Phenol: The Role of Molecular Structure on Interfacial Properties. *Langmuir* **2002**, *18*, 120−126.

(12) Azmi, A. A.; Ebralidze, I. I.; Dickson, S. E.; Horton, J. H. Characterization of Hydroxyphenol-Terminated Alkanethiol Self-Assembled Monolayers: Interactions with Phosphates by Chemical Force Spectrometry. *J. Colloid Interface Sci.* **2013**, *393*, 352−360.

(13) Holten-Andersen, N.; Mates, T. E.; Toprak, M. S.; Stucky, G. D.; Zok, F. W.; Waite, J. H. Metals and the Integrity of a Biological Coating: The Cuticle of Mussel Byssus. *Langmuir* **2009**, *25*, 3323−3326.

(14) Shimada, T. Salivary Proteins as a Defense Against Dietary Tannins. *J. Chem. Ecol.* **2006**, *32*, 1149−1163.

(15) Rahim, M. A.; Kristufek, S. L.; Pan, S.; Richardson, J. J.; Caruso, F. Phenolic Building Blocks for the Assembly of Functional Materials. *Angew. Chem., Int. Ed.* **2019**, *58*, 1904−1927.

(16) Wakasugi, K.; Iida, A.; Misaki, T.; Nishii, Y.; Tanabe, Y. Simple, Mild, and Practical Esterification, Thioesterification, and Amide Formation Utilizing p-Toluenesulfonyl Chloride and N-Methylimidazole. *Adv. Synth. Catal.* **2003**, *345*, 1209−1214.

(17) Smaby, J. M.; Kulkarni, V. S.; Momsen, M.; Brown, R. E. The Interfacial Elastic Packing Interactions of Galactosylceramides, Sphingomyelins, and Phosphatidylcholines. *Biophys. J.* **1996**, *70*, 868−877.

(18) Kaganer, V. M.; Möhwald, H.; Dutta, P. Structure and Phase Transitions in Langmuir Monolayers. *Rev. Mod. Phys.* **1999**, *71*, 779−819.

(19) Jacquemain, D.; Leveiller, F.; Weinbach, S. P.; Lahav, M.; Leiserowitz, L.; Kjaer, K.; Als-Nielsen, J. Crystal Structure of Self-Aggregates of Insoluble Aliphatic Amphiphilic Molecules at the Air-Water Interface. An x-Ray Synchrotron Study. *J. Am. Chem. Soc.* **1991**, *113*, 7684−7691.

(20) Vollhardt, D.; Brezesinski, G. Effect of Chirality on Monoacylglycerol Ester Monolayer Characteristics: 3-Monostearoyl-Sn-Glycerol. *Phys. Chem. Chem. Phys.* **2017**, *19*, 7009−7024.

(21) Kaganer, V. M.; Peterson, I. R.; Kenn, R. M.; Shih, M. C.; Durbin, M.; Dutta, P. Tilted Phases of Fatty Acid Monolayers. *J. Chem. Phys.* **1995**, *102*, 9412−9422.

(22) Vollhardt, D.; Stefaniu, C.; Brezesinski, G. Special Features of Monolayer Characteristics of N-Alkanoyl Substituted Threonine Amphiphiles. *Phys. Chem. Chem. Phys.* **2019**, *21*, 96−103.

(23) Jensen, T. R.; Kjaer, K. Structural Properties and Interactions of Thin Films at the Air-Liquid Interface Explored by Synchrotron X-

DOI: 10.1021/acsami.9b16958
ACS Appl. Mater. Interfaces 2019, 11, 45354−45363

Ray Scattering. In *Novel Methods to Study Interfacial Layers*; Möbius, D., Miller, R., Eds.; Elsevier, 2001; Vol. *11*, pp 205−254.
(24) Yue, X.; Dobner, B.; Iimura, K.-i.; Kato, T.; Möhwald, H.; Brezesinski, G. Weak First-Order Tilting Transition in Monolayers of Mono- and Bipolar Docosanol Derivatives. *J. Phys. Chem. B* **2006**, *110*, 22237−22244.
(25) Durbin, M. K.; Richter, A. G.; Yu, C.-J.; Kmetko, J.; Bai, J. M.; Dutta, P. Backbone Orientational Order in Fatty Acid Monolayers at the Air-Water Interface. *Phys. Rev. E: Stat. Phys., Plasmas, Fluids, Relat. Interdiscip. Top.* **1998**, *58*, 7686−7690.
(26) Boehm, C.; Leveiller, F.; Jacquemain, D.; Moehwald, H.; Kjaer, K.; Als-Nielsen, J.; Weissbuch, I.; Leiserowitz, L. Packing Characteristics of Crystalline Monolayers of Fatty Acid Salts, at the Air-Solution Interface, Studied by Grazing Incidence X-Ray Diffraction. *Langmuir* **1994**, *10*, 830−836.
(27) Pascher, I.; Sundell, S. Molecular Arrangements in Sphingolipids. The Crystal Structure of Cerebroside. *Chem. Phys. Lipids* **1977**, *20*, 175−191.
(28) Stefaniu, C.; Vilotijevic, I.; Brezesinski, G.; Seeberger, P. H.; Varón Silva, D. Varón Silva, D. A Comparative Structural Study in Monolayers of GPI Fragments and Their Binary Mixtures. *Phys. Chem. Chem. Phys.* **2014**, *16*, 9259−9265.
(29) Stefaniu, C.; Vilotijevic, I.; Santer, M.; Varón Silva, D.; Brezesinski, G.; Seeberger, P. H. Subgel Phase Structure in Monolayers of Glycosylphosphatidylinositol Glycolipids. *Angew. Chem., Int. Ed.* **2012**, *51*, 12874−12878.
(30) Dwibedy, P.; Dey, G. R.; Naik, D. B.; Kishore, K.; Moorthy, P. N. Pulse Radiolysis Studies on Redox Reactions of Gallic Acid: One Electron Oxidation of Gallic Acid by Gallic Acid−OH Adduct. *Phys. Chem. Chem. Phys.* **1999**, *1*, 1915−1918.
(31) Eslami, A. C.; Pasanphan, W.; Wagner, B. A.; Buettner, G. R. Free Radicals Produced by the Oxidation of Gallic Acid: An Electron Paramagnetic Resonance Study. *Chem. Cent. J.* **2010**, *4*, 15.
(32) Huguenin, J.; Ould Saad Hamady, S.; Bourson, P. Monitoring Deprotonation of Gallic Acid by Raman Spectroscopy. *J. Raman Spectrosc.* **2015**, *46*, 1062−1066.
(33) Kumar, J. K.; Oliver, J. S. Proximity Effects in Monolayer Films: Kinetic Analysis of Amide Bond Formation at the Air−Water Interface Using 1H NMR Spectroscopy. *J. Am. Chem. Soc.* **2002**, *124*, 11307−11314.
(34) Seul, M.; Andelman, D. Domain Shapes and Patterns: The Phenomenology of Modulated Phases. *Science* **1995**, *267*, 476−483.
(35) McConnell, H. M. Theory of Hexagonal and Stripe Phases in Monolayers. *Proc. Natl. Acad. Sci. U.S.A.* **1989**, *86*, 3452−3455.
(36) Melzer, V.; Vollhardt, D.; Weidemann, G.; Brezesinski, G.; Wagner, R.; Möhwald, H. Structure Formation and Phase Transitions in Gibbs and Langmuir Monolayers of Amphiphilic Acid Amides. *Phys. Rev. E: Stat. Phys., Plasmas, Fluids, Relat. Interdiscip. Top.* **1998**, *57*, 901−907.
(37) Hossain, M. M.; Iimura, K.-i.; Kato, T. Temperature and Compression Rate Independent Domain Shape in Langmuir Monolayers of Di-n-Dodecyl Hydrogen Phosphate at the Air−water Interface. *J. Colloid Interface Sci.* **2008**, *319*, 295−301.
(38) Flores, A.; Ize, P.; Ramos, S.; Castillo, R. The Dioctadecylamine Monolayer: Textures, Phase Transitions, and Dendritic Growth. *J. Chem. Phys.* **2003**, *119*, 5644−5653.
(39) Hoffmann, F.; Stine, K. J.; Hühnerfuss, H. Appearance and Disappearance of Dendritic and Chiral Patterns in Domains of Langmuir Monolayers Observed with Brewster Angle Microscopy. *J. Phys. Chem. B* **2005**, *109*, 240−252.
(40) Davies, J. T.; Rideal, E. K. Properties of Monolayers. In *Interfacial Phenomena*; Davies, J. T., Rideal, E. K., Eds.; Academic Press, 1961; Chapter 5, pp 217−281.
(41) Vollhardt, D.; Emrich, G.; Siegel, S.; Rudert, R. Phase Transition in Monolayers of Straight Chain and 2-Methyl Branched Alcohols at the Air−Water Interface. *Langmuir* **2002**, *18*, 6571−6577.
(42) Fainerman, V. B.; Vollhardt, D.; Johann, R. Arachidic Acid Monolayers at High PH of the Aqueous Subphase: Studies of Counterion Bonding. *Langmuir* **2000**, *16*, 7731−7736.
(43) Johann, R.; Vollhardt, D. Texture Features of Long-Chain Fatty Acid Monolayers at High PH of the Aqueous Subphase. *Mater. Sci. Eng., C* **1999**, *8-9*, 35−42.
(44) Ghaicha, L.; Chattopadhyay, A. K.; Tajmir-Riahi, H. A. Behavior of Stearic Acid Monolayers in Presence of Concentrated Ammonium Nitrate Solution Substrate. *Langmuir* **1991**, *7*, 2007−2009.

DOI: 10.1021/acsami.9b16958
ACS Appl. Mater. Interfaces 2019, 11, 45354−45363